Fluorescence mechanism switching from ICT to PET by substituent chemical manipulation: Macrophage cytoplasm imaging probes

Francisco Fueyo-González[a], Juan A. González-Vera[a,b,*], Ibon Alkorta [a], Lourdes Infantes[c], M. Luisa Jimeno[d], Mar Fernández-Gutiérrez[e], M. Carmen González-García[b], Angel Orte[b], Rosario Herranz[a,*]

[a]*Instituto de Química Médica (CSIC). Juan de la Cierva 3, 28006 Madrid, Spain.*

[b]*Departamento de Fisicoquímica, Unidad de Excelencia de Química aplicada a Biomedicina y Medioambiente, Facultad de Farmacia, Universidad de Granada, Campus Cartuja, 18071, Granada, Spain.*

[c]*Instituto de Química Física Rocasolano, IQFR-CSIC. Serrano 119, 28006 Madrid, Spain.*

[d]*Centro de Química Orgánica Lora Tamayo (CSIC). Juan de la Cierva 3, 28006 Madrid, Spain.*

[e]*Instituto de Ciencia y Tecnología de Polímeros (CSIC), CIBER-BBN, Juan de la Cierva 3, 28006 Madrid, Spain.*

ABSTRACT

The lack of polarity sensing fluorophores with OFF-ON features when increasing the environment polarity has limited the monitoring of biological processes that involve an increase in local hydrophilicity. In this work, replacement of a hydroxyl group by a dimethylamino group transformed solvatochromic ICT naphthalimide- and quinolimide-based fluorophores into reversed solvatochromic ones, with higher emission in polar than in apolar environments. Excited-state dynamics studies, TD-DFT calculations, X-ray and NMR support the existence of a folded conformation for the 2-(dimethylamino)ethyl chain upon the imide ring in apolar solvents, where the dimethylamino group

[*]Corresponding authors.
E-mail addresses: rosario@iqm.csic.es (R. Herranz); gonzalezvera@ugr.es (J. A. González-Vera)

22 would quench the fluorescence by a PET effect, while in polar solvents the chain has an extended

23 conformation, where the PET is hindered. These PET fluorophores have given rise to H_2O and pH

24 sensors in organic solvents as well as to bright macrophage cytoplasm imaging probes.

25

28

1. Introduction

30 The 1,8-naphthalimide scaffold is found among the most fruitful structures in the design of

31 fluorophores with application in the development of fluorescence biosensors, due to its small size and

32 the ease of tuning the photophysical properties by manipulating its substitution pattern. Thus,

33 naphthalimide-based fluorophores have found application in pH[1-3], cation[4] and anion[5]

34 chemosensors, DNA binders and anticancer agents[5, 6] or in biomolecular interaction sensors[7-9]

35 and cellular imaging agents[6, 8, 10]. Since introduction of a protonatable nitrogen atom into the 1,8-

36 naphthalimide skeleton could red-shift the fluorescence emission and increase water solubility, we

37 have recently studied and reported the synthesis and photophysical properties of a series of 9-

38 methoxy-quinolimide analogues[11]. These compounds resulted in highly solvatochromic

39 fluorophores, based on an intramolecular charge transfer (ICT) mechanism.

40 In contrast to the abundance of ICT-based probes for polarity sensing, that exhibit a marked

41 decrease in their fluorescence (ON-OFF) upon increasing environment polarity, the number of polarity

42 OFF-ON sensors is very limited. The scarcity of this type of fluorophores has limited the monitoring

43 of biological processes that involve an increase in local polarity and justifies the interest of these

44 probes. Taking into account these precedents, we have studied the effect of introducing a 2-

45 (dimethyl)aminoethyl moiety, able to quench fluorescence by photoinduced electron transfer (PET) [1,

46   4, 5, 12, 13], into the imide group of naphthalimide (**1a**) and quinolimide (**1b**) scaffolds (Figure 1) and

47   their comparison with analogues carrying a 2-(hydroxy)ethyl chain **2a** and **2b**. We have also studied

48   their applicability for *in cellulo* imaging in macrophages, obtaining bright cell cytoplasm dyes.
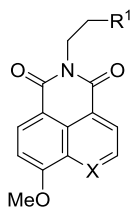
a: X = CH; **b**: X = N
1a and **1b**: R^1 = NMe_2
2a and **2b**: R^1 = OH

49   **Figure 1**. Naphthalimides **1a** and **2a** and quinolimide analogues **1b** and **2b**.

50   **2.   Experimental Section**

51   *2.1. General chemical methods*

52   All reagents were of commercial quality. Solvents were dried and purified by standard methods.

53   Analytical TLC was performed on aluminum sheets coated with a 0.2 mm layer of silica gel 60 F_{254}.

54   Silica gel 60 (230-400 mesh) was used for flash chromatography. HPLC-MS was performed on a

55   Sunfire C_{18} (4.6×50 mm, 3.5 μm) column at 30°C, with a flow rate of 1 mL/min and gradient of 0.1%

56   of formic acid in CH_3CN (solvent A) in 0.1% of formic acid in H_2O (solvent B) was used as mobile

57   phase. Electrospray in positive mode was used for ionization. NMR spectra were recorded using

58   Varian Inova or Mercury 400, and Varian Unity 500 spectrometers. The NMR spectra assignments

59   were based on COSY, HSQC, and HMBC spectra. High resolution mass spectra (HRMS) were

60   recorded on an Agilent 6520 Q-TOF instrument with an ESI source. MW experiments were carried out

61   in sealed vessels in a MW Emrys™ Synthesizer (Biotage AB), with transversal IR sensor for reaction

62   temperature monitoring. UV-visible spectroscopy measurements were made at 25 Cº on a Lambda 35,

63   Perkin Elmer, UV-vis spectrophotometer; Starna Cells (16.100-Q-10) 100 μL sub-micro cuvette, 1 cm

64   path length. Steady-state fluorescence emission spectra were performed at 25 Cº either on a

65   PerkinElmer LS 50B luminescence spectrometer or a JASCO FP-8300 spectrofluorometer equipped

66 with a 450 W xenon lamp for excitation; Starna Cells (16.100F-Q-10) 100 μL sub-micro cuvette, 1 cm

67 path length.

68 *2.2. Synthesis of 5-(2-(dimethylamino)ethyl)-9-methoxy-4H-benzo[*de*]/[2,6]naphthyridine-4,6(5H)-*

69 *dione* (**1b**)

70 *N,N*-dimethylethylenediamine (26 μL, 0.24 mmol) was added to a solution of 9-methoxy-4*H*,6*H*-

71 pyrano[3,4,5-*de*]quinoline-4,6-dione[11] (**3b**) (180 mg, 0.78 mmol) in EtOH (3mL), and this mixture

72 was heated at 120 ºC under MW irradiation for 1.5 h. Afterwards, the solvent was evaporated to

73 dryness and the residue was purified by flash chromatography, using 5-25% gradient of MeOH in

74 CH$_2$Cl$_2$ as eluent, to give the desired quinolimide **1b** as a yellow solid (140 mg, 61 %). M.p. 142 ºC.

75 HPLC-MS (30-95% gradient of A in B, 10 min) t_R = 3.08 min. ^{1}H-NMR (Cl$_3$CD, 400 MHz) δ: 2.29 [s,

76 6H,], 2.60 (t, 2H, *J* = 6.5 Hz), 4.15 (s, 3H), 4.24 (t, 2H, *J* = 6.5 Hz), 7.21 (d, 1H, *J* = 8.5 Hz), 8.27 (d,

77 1H, *J* = 4.5 Hz), 8.51 (d, 1H, *J* = 8.5 Hz), 9.14 (d, 1H, *J* = 4.5 Hz). ^{13}C-NMR (Cl$_3$CD, 100 MHz) δ:

78 38.3, 45.8, 56.9, 57.0, 108.8, 114.7, 123.1, 124.2, 129.7, 133.6, 139.0, 150.5, 160.7, 162.9, 163.5.

79 HRMS (ESI) *m/z*: Calc. for C$_{16}$H$_{17}$N$_3$O$_3$ ([M+H]$^+$): 300.1270, Found: 300.1272.

80 2.3. *Photophysical methods*

81 *2.3.1. Determination of steady-state photophysical properties*

82 Excitation and emission spectra of compounds were determined for 12 μM solutions in solvents of

83 diverse polarity. The spectra were recorded between 300 and 690 nm (0.5 nm increments and 0.1 s

84 integration time) with excitation set at the appropriate excitation wavelength. Slit widths were set to 15

85 nm for excitation and to 6 or 20 nm for emission, depending on the observed emission intensity. All

86 the spectra were corrected for background fluorescence by subtracting a blank scan of the solvent

87 solution.

88 *Fluorescence quantum yield determination*. Fluorescence quantum yields (Φ_F) were determined in

89 solvents of different polarity. Quinine sulphate dihydrate in 0.1 M H$_2$SO$_4$ (Φ_F = 0.55) was used as a

90 reference. A 12 μM solution of the corresponding fluorophore was compared to a 12 μM solution of

91 the standard to assure that the absorbance is less than 0.1 at identical excitation wavelengths. The

92 following equation (E1) was used to calculate the quantum yield:

$$\Phi = \frac{I_x A_r n^2{}_x \Phi_r}{A_x I_r n^2{}_r}$$

93 (E1)

94 where x and r denote the sample and standard, respectively, A is the absorption at the excitation

95 wavelength, I is the integrated fluorescence intensity, and n is the refractive index of the solvent.

96 Cross-calibration between standards yielded less than 10% error for this method and instrumentation.

97 *2.3.2. Time-resolved fluorimetry*

98 Fluorescence decay traces were recorded using a FluoTime 200 time-resolved spectrofluorimeter

99 (PicoQuant, Germany) with a pulsed diode laser 375 nm (LDH-375, PicoQuant) working at 10 MHz

100 of repetition rate. Time resolved Emission Spectra (TRES) is a valuable tool that allow obtain the

101 emission spectra of compounds with time resolution, which mean reconstruct the emission spectra for

102 each single time in nanosecond scale. To obtain TRES we recorded decay traces from 395 to 530 nm

103 with $\Delta\lambda = 3$ nm. Decay traces were fitted to one or two exponential decay components after correction

104 of the traces for the same instrumental and acquisition time conditions. Finally, TRES spectra were

105 calculated using equation E2 for total times of 0, 0.5, 0.8, 1, 1.2, 1.5, 3, 5, 8, 10 and 15 nanoseconds.

106 $$I_\lambda(t) = \sum_{i=1}^{n} p_i \cdot e^{-t/\tau_i} \qquad (E2)$$

107 where I_λ (t) is the time-dependent fluorescence intensity at each wavelength, *n* is the number or

108 exponential decay components, p_i is the amplitude of each decay component at λ wavelength and τ_i is

109 the lifetime of each component.

110 The species-associated emission spectra (SAEMS) represent the spectral contribution of each

111 species *i* to the global fluorescence spectrum. The SAEMS are estimated by equation E3, where $I_{ss,\lambda}$ is

112 the corrected fluorescent intensity in the steady-state.

113
$$I_{i,\lambda} = \frac{p_i \cdot \tau_i}{\sum_{i=1}^{n} p_i \cdot \tau_i} I_{SS,\lambda} \qquad \text{(E3)}$$

114

115   2.4. *Computational methods*

116   TD-DFT calculations have been carried out at the PBE0/6-31+G(d,p) computational level[14, 15],

117 within the Gaussian-09 package[16]. In order to explore the conformation profile of the side chain of

118 **1a,b** and **2a,b**, nine starting points have been considered by 120º rotation of the C1'-C2' and C2'-O/N

119 bonds. The rotation around the N-C1' bond has not been considered since only two conformations are

120 possible that provide enantiomeric conformations. The solvent effect has been taken into account with

121 the PCM continuum model[17] and the parameters for cyclohexane, acetone and water. In all cases,

122 frequency calculations have been carried out to confirm that the geometries obtained corresponded to

123 energetic minima. In addition, the geometry of the conformers has been optimized in the first excited

124 stated with the TD-DFT methodology in gas phase.

125   The electron density differences between ground and excited states have been obtained with the

126 Gaussian-09 facilities and displayed with the Jmol program[18].

127   2.5. *X-Ray Diffraction of 1a*

128   Many low-quality crystals of compound **1a** were mounted and tested on a Bruker APEX-II CCD

129 diffractometer until a suitable needle shape crystal was collected at 120K. Using Olex[19], the

130 structure was solved with the ShelXS [20] structure solution program using Direct Methods and

131 refined with the ShelXL [21] refinement package using Least Squares minimisation.

132   Crystal Data for **1a** ($C_{17}H_{18}N_2O_3$, M =298.33 g/mol): monoclinic, space group P2/c (no. 13), a =

133 7.1171(2) Å, b = 13.7950(4) Å, c = 15.1220(5) Å, β = 98.8826(17)°, V = 1466.88(8) Å^3, Z = 4, T =

134 120.0 K, μ(CuKα) = 0.763 mm^{-1}, $Dcalc$ = 1.351 g/cm^3, 32021 reflections measured (6.406° $\leq$ 2Θ $\leq$

135 124.84°), 2303 unique (R_{int} = 0.1252, R_{sigma} = 0.0576) which were used in all calculations. The final R_1

136 was 0.0724 (I > 2σ(I)) and wR_2 was 0.1933 (all data). CCDC 1954522 contains the supplementary

137 crystallographic data for compound **1a**. These data can be obtained free of charge from the Cambridge

138 Crystallographic Data Centre[22].

139 2.6. *Macrophage Culture and Fluorescence Visualization*

140   Macrophages RAW 264.7 (ECACC, Sigma P11) were used for testing naphthalimides **1a,2a** and

141 quinolimides **1b,2b** as imaging probes. The cells were cultured in Dulbecco's modified Eagle's

142 medium enriched with 100 mg/L of sodium piruvate supplemented with 10% fetal bovine serum

143 (FBS), 200 mM L-glutamine, 100 u/mL penicillin and 100 μg/mL of streptomycin (complete

144 medium). The cell culture was maintained in humidified atmosphere at 37 ºC, with 5 % of CO_2 and 95

145 % of air. The morphology of the cells was studied with an epifluorescence microscope Nikon TE-2000

146 and with the confocal Laser microscope (CLSM) LEICA TCS SP2 with 7 lines of laser (457, 477, 488,

147 496, 514, 543, 633 nm).

148   RAW 264.7 cells were grown to a density of 8 x 10^4 cells/mL in complete medium, in 24-well

149 plates incubated for 24 hours. After this time, half of the growing wells were treated with LPS

150 (Polysaccharides of Escherichia coli, Sigma Aldrich, Spain) at a concentration of 5 μg/mL for 2 h and,

151 then, treated with the corresponding fluorophore (5 μM). The other half of the wells were treated

152 directly with the flourophore at the same concentration. The cells were left in the presence of the dyes

153 for 1 or 2 h. After this time, the cells were fixed with glutaraldehyde (2.5% v/v in H_2O) for 15

154 minutes. They were washed with distilled water twice and mounted and observed under the

155 microscope. The images of cells treated with our products were compared with images obtained with

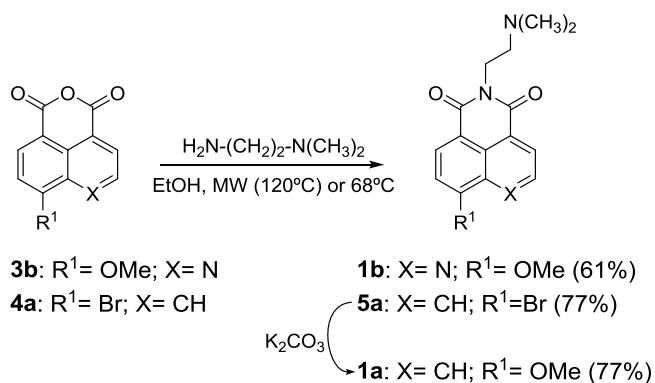156 the commercial nuclear fluorescent sensor DAPI (Invitrogen[®]).

157

158 **3. Results and discussion**

159 *3.1. Synthesis*

160   As shown in Scheme 1, the 5-[2-(dimethylamino)ethyl]-quinolimide **1b** was synthesized from the

161 corresponding anhydride **3b**[11] (Scheme 1) by reaction with *N,N*-dimethylethylenediamine, while the

162 2-[2-(dimethylamino)ethyl]-naphthalimide **1a** [23] was obtained from the commercially available 4-

163 bromo-1,8-naphthalic anhydride **4a**, by reaction also with *N,N*-dimethylethylenediamine, followed by

164 treatment with K_2CO_3 in refluxing MeOH. The 2-(hydroxy)ethyl analogues **2a** and **2b** were obtained

165 as previously described[11].

3b: R^1= OMe; X= N
4a: R^1= Br; X= CH

1b: X= N; R^1= OMe (61%)
5a: X= CH; R^1=Br (77%)
1a: X= CH; R^1= OMe (77%)

H_2N-$(CH_2)_2$-$N(CH_3)_2$
EtOH, MW (120ºC) or 68ºC

K_2CO_3

166 **Scheme 1.** Synthesis of the naphthalimide **1a** and the quinolimide **1b**

167

168 *3.2. Photophysical properties*

169   The absorption and emission spectra of **1a,b** and **2a,b** were registered in solvents of varying

170 polarity and the more significant photophysical data are shown in Table 1. The data show that the

171 variation at the R^1 substituent does not affect to the absorption and emission wavelengths, which

172 display bathochromic shifts with increasing solvent polarity (30-48 nm in λ_{max}^{em} from $CHCl_3$ to H_2O),

173 but it affects significantly to the extinction coefficients (ε) and to the fluorescence quantum yields (Φ_F)

174 and, therefore, to the fluorescence brightness. While compounds carrying the 2-(hydroxyl)ethyl chain,

175 **2a** and **2b,** showed a clear solvatochromic behavior, with decreasing Φ_F when the solvent polarity

176 increases, in the compounds carrying the 2-(dimethylamino)ethyl chain, **1a** and **1b,** Φ_F increased with

177 the solvent polarity and, particularly, with its acidity, such as in trifluoroethanol. Thus, as shown in

178 Figure 2, the fluorescence intensity increased 22-fold and 14-fold from CH_3CN to H_2O solution for the

179 naphthalimide **1a** and quinolimide **1b** derivatives, respectively. This striking contrasting behavior

180 must be related to differences in the solvent effects over the excited-state dynamics of these dyes.

181 **Table 1.** Photophysical properties of the naphthalimide and quinolimide derivatives **1a,b** and **2a,b**

Compd[a]	Solvent	λ_{max}^{abs} (nm)	ε ($M^{-1}cm^{-1}$)	λ_{max}^{em} (nm)	Φ_F[b]
	CHCl₃	366	8100	428	0.20
	Dioxane	358	6700	425	0.22
	Acetone	359	9700	433	0.14
1a	EtOH	366	7100	434	0,25
	F₃C-CH₂OH	371	10100	450	0.63
	MeOH	367	8300	444	0.50
	H₂O[c]	376	7200	460	0.63
	CHCl₃	377	3100	457	0.12
	Dioxane	367	2800	457	0.17
	Acetone	370	4900	467	0.04
1b	EtOH	375	3300	475	0.09
	F₃C-CH₂OH	380	2900	495	0.63
	MeOH	376	3700	493	0.23
	H₂O[c]	381	3200	505	0.26
	CHCl₃	360	14540	428	0.57
	Dioxane	359	12080	426	0.60
	Acetone	357	13610	434	0.43
2a	EtOH	364	12120	439	0,60
	F₃C-CH₂OH	373	11950	449	0.32
	MeOH	366	12790	442	0.57
	H₂O[c]	375	9650	458	0.30
	CHCl₃	378	8900	457	0.68
	Dioxane	372	8600	460	0.67
	Acetone	371	8170	468	0.56
2b	EtOH	375	7221	485	0.36
	F₃C-CH₂OH	379	7870	488	0.29
	MeOH	375	6760	490	0.27
	H₂O[c]	381	8220	500	0.16

182 [a]Measured in duplicate at a 12 μM concentration. [b]Quantum yields calculated with reference to quinine sulfate (in 0.1 M
183 H₂SO₄). [c]H₂O with 10% of MeOH.

184

185   The behavior of the quinolimide derivatives **1b** and **2b** was similar to that of the naphathalimide

186   analogues **1a** and **2a**, except for the bathochromic shifts in the absorption and emission maxima of the

187   quinolimide derivatives (5-12 nm in λ_{max}^{abs} and 30-50 nm in λ_{max}^{em}) and the higher solvatochromic

188   behavior of the quinolimide **2b** than the naphthalimide **2a**.
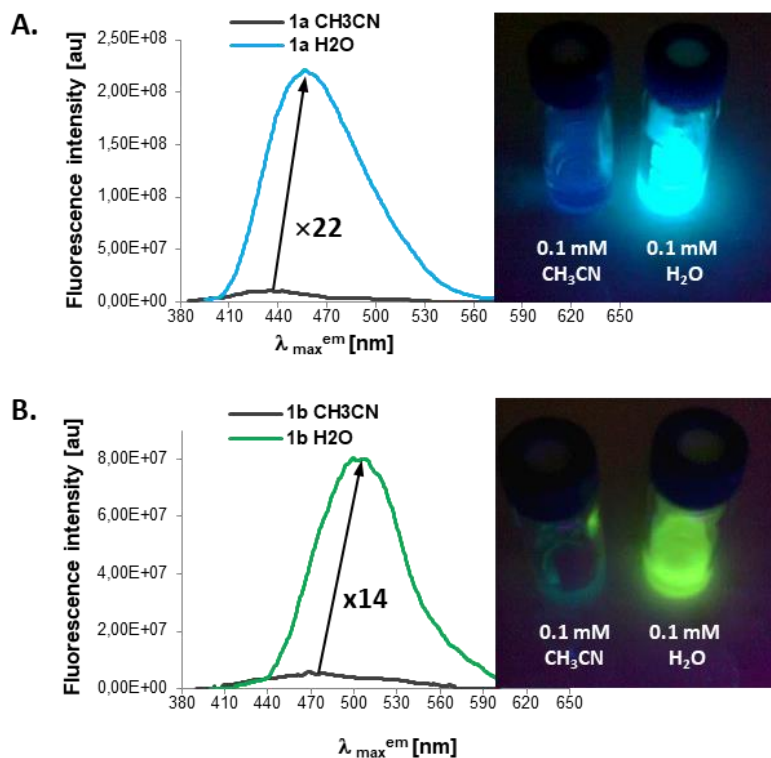
Figure 2. Emission spectra and fluorescence image of **1a** (A) and **1b** (B) upon UV lamp irradiation (λ_{ex} = 365 nm) in CH$_3$CN and H$_2$O.

189   To explain the effect of solvent on the photophysical properties ($\tilde{\nu}_{abs}$ and $\tilde{\nu}_{em}$ and Φ_F) of **1a,b** and

190   **2a,b**, we applied the multilinear equation of J. Catalán [24] [$y = y_0 + a_{SA}SA + b_{SB}SB + c_{SP}SP +$

191     $d_{SdP}SdP$], which uses four empiric scales of solvent effects: dipolarity (SdP), polarizability (SP),

192   acidity (SA) and basicity (SB). For this purpose, we determined the absorption and emission

193   frequencies and Φ_F in 10 diverse solvents (CHCl$_3$, CH$_2$Cl$_2$, 1,4-dioxane, THF, acetone, isopropanol,

194   EtOH, MeOH, H$_2$O and trifluoroethanol). The multi-linear analysis of the results, using the four

195   solvent scales, gave good correlation coefficients (r>0.9) for the absorption and emission frequencies

196   and showed a main and negative contribution of the acidity coefficient (a_{SA}) (Table 2) for all the four

197   compounds. This negative value would explain the bathochromic shifts observed increasing the

198   solvent acidity. Regarding the quantum yields, the results were more diverse. In the 5-[2-

199 (hydroxyl)ethyl]quinolimide derivative **2b**, the analysis showed a clear and negative effect of the

200 solvent acidity on the Φ_F value, in agreement with its clear solvathocromic behavior. For the other

201 compounds no clear correlations were obtained.

202 **Table 2**. Regression coefficients of the Catalán equation applied to study the influence of solvent properties on
203 the photophysical properties of **1a,b** and **2a,b**, calculated by the multilinear regression $[y = y_0 + a_{SA}SA + b_{SB}SB$
204 $+ c_{SP}SP + d_{SdP}SdP]$.

Compd	y	y_0	a_{SA}	b_{SB}	c_{SP}	d_{SdP}	r
	$\tilde{v}_{abs}$ (cm^{-1})	29770±1063	-990±232	13±257	-2462±1225	-549±359	0.9591
1a	$\tilde{v}_{em}$ (cm^{-1})	24306±955	-1225±208	12±231	-628±1101	-741±323	0.9847
	Φ_F	0.550±0.487	0.468±0.106	-0.031±0.118	-0.387±0.561	-0.142±0.164	0.9654
	$\tilde{v}_{abs}$ (cm^{-1})	31877±1147	-1439±299	-96±226	-5848±1302	-1095±322	0.9501
1b	$\tilde{v}_{em}$ (cm^{-1})	23376±1892	-1761±493	-853±373	-1191±2147	-845±531	0.9696
	Φ_F	1.986±0.556	0.082±0.114	-0.497±0.129	-1.917±0.556	-0.435±0.180	0.9344
	$\tilde{v}_{abs}$ (cm^{-1})	30136±1532	-1532±400	-100±302	-2937±1738	-259±430	0.9296
2a	$\tilde{v}_{em}$ (cm^{-1})	22895±495	-736±129	22±98	1035±562	-568±139	0.9948
	Φ_F	1.038±1.053	-0.099±0.240	-0.082±0.270	-0.513±1.168	-0.245±0.378	0.3905
	$\tilde{v}_{abs}$ (cm^{-1})	29068±735	-875±192	162±145	-2986±833	-290±206	0.9526
2b	$\tilde{v}_{em}$ (cm^{-1})	22415±618	-1473±161	-1169±122	65±702	-587±173	0.9968
	Φ_F	1.009±0.210	-0.479±0.048	-0.275±0.054	-0.225±0,233	-0.165±0.075	0.9920

205

206

207 *3.3. Hindering PET quenching by solvent acidity*

208   With the aim of elucidating the different mechanisms of fluorescence of the 2-

209 (dimethylamino)ethyl derivatives **1a,b** from the corresponding 2-(hydroxy)ethyl analogues **2a,b**, we

210 carried out further time-resolved fluorimetry measurements, TD-DFT calculations, and NMR and X-

211 ray diffraction studies as follows.

212   First, we tested the excited-state dynamics of **1a** by following the fluorescence decay traces, using

213 time-resolved fluorimetry. When dissolved in water, **1a** exhibited strictly mono-exponential decay

214   traces, with a fluorescence lifetime of 9.99 ± 0.03 ns. In contrast, **1a** dissolved in other organic

215   solvents, such as chloroform, presented two decay components: a long decay time of 7.11 ± 0.02 ns

216   and a short decay time of 2.69 ± 0.02 ns. Interestingly, the short decay time was a rise-time, with

217   negative pre-exponential factor at wavelengths above 476 nm. Negative pre-exponential factors are

218   unequivocally indicative of a reaction in excited-state, by which a more fluorescent species is formed

219   from the initially excited form, during the time of such excited state. We then performed time-resolved

220   emission spectroscopy (TRES) of **1a** in chloroform to extract the whole spectral information related to

221   these dynamics. Figure 3A shows how the emission spectra of **1a** changed with time during the

222   excited state.
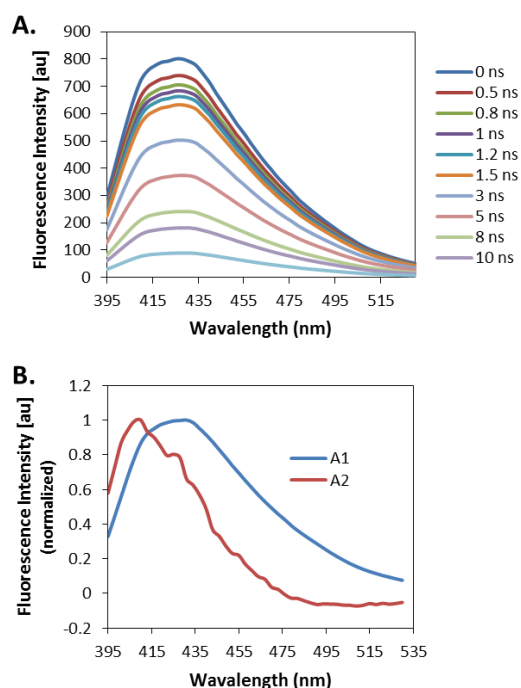
Figure 3. (A) TRES spectra of **1a** in chloroform (λ_{ex} = 375 nm) in a time window between 0 and 15 ns after the excitation pulse. (B) Corresponding SAEMS of the long (blue) and short (red) decay components.

223   When analyzing the species-associated emission spectra (SAEMS) of the two decay components

224   (Figure 3B, A1 and A2) the spectrum associated with the short-lived component (A2) clearly showed a

225   negative contribution at long wavelengths. This confirms that the initially excited form undergoes a

226   transformation to a red-shifted, more fluorescent species. In the context of an excited-state reaction,

227   we can establish that a transformation occurred within 2.69 ns, which gave rise to a red-shifted species

228   from the blue-shifted form (Scheme 2). The spectral features of the appearing form were similar to

229 those found in acidic solvents, such as water and methanol (higher quantum yield and red-shift

230 emission, see Table 1). Importantly, chloroform has certain acidic behavior. For instance, the acidity

231 parameter for chloroform in the solvent scale proposed by Catalán is 0.047[24]. Even though it is a

232 small value, this means that the solvent has a certain ability to withdraw electrons and to form

233 hydrogen bonding. The low acidity of the solvent could also explain why the excited-state reaction did

234 not proceed extensively, and it was only detected with a low contribution. In any case, these kinetics

235 suggested the coexistence of two different emitters, depending on the acidity properties of the solvent.
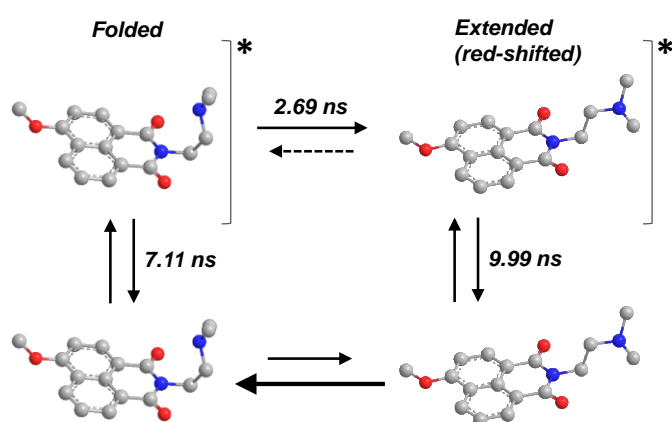
Scheme 2. The two-state excited-state kinetic system applied to the dynamics of **1a** dissolved in chloroform.

236 The 2-(dimethylamino)ethyl modified naphthalimide, **1a**, showed simple kinetics that could be

237 resolved with reasonable assumptions. In contrast, the corresponding quinolimide, **1b**, exhibited more

238 complex excited-state dynamics, with three different decay components, even in aqueous solution.

239 This is probably due to the additional acid-base interaction that the electron pair in the N of the

240 quinolimide moiety, and the presence of additional prototropic forms in equilibrium (see below). In

241 any case, the conclusions drawn for the study of **1a**, regarding the 2-(dimethylamino)ethyl radical

242 could be extrapolated to **1b**, since that part of the molecule is equivalent in both dyes.

243 To gain more insights into the nature of these species and to confirm the influence of the solvent's

244 acidity, we performed TD-DTF calculations at the PBE0/6-31+G(d,p) computational level[25, 26]

245 within the Gaussian-09 software [16]. The geometry of the ground (GS) and first singlet excited (ES)

246 electronic states of all the studied dyes was optimized in vacuum and in solvents of different polarity

247 (cyclohexane, acetone, and H_2O). The model of continuous solvent PMC and the corresponding

248 parameters[17] were used for the calculations with solvent. With the aim of exploring the

249 conformational differences between the 2-(hydroxy)ethyl- and 2-(dimethylamino)ethyl- derivatives,

250 we used as starting points of the analysis 9 conformations corresponding to 120º rotations around the

251 C-C and C-O/N bonds of the chain. Frequencies were calculated in all cases to confirm that the

252 obtained geometries corresponded to energy minima. Three conformations of minimum energy were

253 obtained for the 2-(hydroxy)ethyl- derivatives **2a** and **2b**, two of them with the chain folded towards

254 the naphthalimide or quinolimide rings, with a hydrogen bond between the OH group of the chain and

255 the C_3 or C_6 carbonyl group of their respective imide ring, with small differences in the hydrogen bond

256 distance and the hydroxyl group bond angle. The conformation with the longest hydrogen bond

257 distance was the energy minimum in gas phase, while that with the shortest hydrogen bond was the

258 energy minimum in solution. In the third minimum, the chain is folded with the hydrogen bond formed

259 between the OH and the respective C_1 or C_4 carbonyl group of the imide ring (Supplementary

260 Material, Figure S1, conformations A, B and C and Table S1 for the quinolimide **2b**).

261 Four minima were obtained in the case of the 2-(dimethylamino)ethyl- derivatives **1a** and **1b**. Both

262 in gas phase and in solution, the two more stable conformations have the 2-(dimethylamino)ethyl

263 chain folded towards the imide ring above each one of the carbonyl groups, with the free electron pair

264 of the nitrogen oriented towards the respective carbonyl group and with a 3.38 Å distance between that

265 nitrogen and those carbon atoms (Supplementary Material, Figures S2 and S3 and tables S2 and S3).

266 The two other minima, which only differ in the relative orientation of the OMe group, corresponded to

267 conformations with the 2-(dimethylamino)ethyl chain extended, which move the dimethylamino group

268 away from the imide ring. In gaseous phase the energy of these two extended conformations was 3.14-

269 3.76 kJ/mol higher than that of the folded conformations, while in solution this energy difference

270 decreased with the solvent polarity in the way that in H_2O it was ≤ 0.7 kJ/mol. The higher stability of

271 the folded conformations in gaseous phase and non-polar solvents would explain the inhibition of

272   fluorescence by a PET effect in these solvents, while in polar solvents, without conformational

273   preference, there is not a PET. These structural calculations could be confirmed experimentally with

274   X-ray diffraction experiments, at least for **1a**. We could obtain good crystal only for the 2-[2-

275   (dimethylamino)ethyl]-naphthalimide **1a** in cyclohexane. Its X-ray diffraction analysis showed

276   molecular coordinates (Figure 4) similar to those obtained in the TD-DFT conformational analysis.

277   The distance between the nitrogen side chain and the carbonyl carbon C_1 was 3.47 Å, very similar to

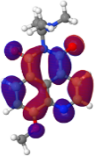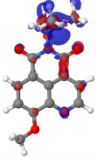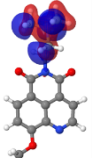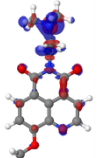278   that measured in the calculations in gaseous phase or non-polar solvent.
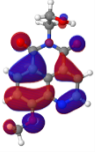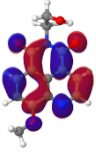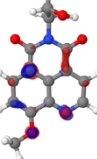

1a
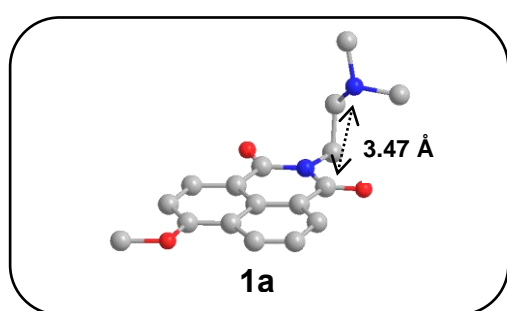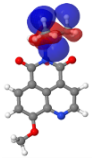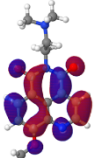
Figure 4. X-ray structure of the 1-(2-(dimethylamino)ethyl)-naphthalimide derivative **1a**

279   The energy and molecular distribution of the frontier orbitals HOMO and LUMO of **1a,b** and

280   **2a,b**, as well as the charge density differences between the ground (GS) and the first singlet excited

281   electronic (ES) state produced by vertical excitation, were also calculated and the results for the

282   quinolimide derivatives **1b** and **2b** are shown in Table 3. In the fluorophores carrying the 2-

283   (hydroxy)ethyl chain, **2a** and **2b**, both the HOMO and LUMO orbitals are mainly localized at the OMe

284   group and at the aromatic ring. The charge losses are localized at the OMe oxygen, the C_{3a} and C_5 in

285   the naphthalimide **2a**, and N_1, C_{6a} and C_8 in the quinolimide **2b**, while charge increases are localized at

286   C_1, C_4 and C_{9a} in **2a** and at C_{3a}, C_4 and C_7 in **2b**. However, in the fluorophores carrying the 2-

287   (dimethylamino)ethyl chain, **1a** and **1b**, the HOMO orbital is mainly localized at this chain, while the

288   LUMO is localized at the aromatic ring and the OMe group. The charge losses are localized at the

289   (dimethylamino)ethyl chain, centered at the nitrogen, and at the N_1 in the quinolimide **1b**. The charge

290   increases are localized at both imide oxygens and C_1, C_9 and C_{9a} in the naphthalimide **1a** and C_3, C_{3a}

291   and C_4 in the quinolimide **1b**. Therefore, all these results would explain the PET effect in the 2-

292 (dimethylamino)ethyl derivatives in non-polar solvents and the different fluorescent behavior with

293 respect to that of the 2-(hydroxyl)ethyl analogues.

Table 3. HOMO and LUMO orbitals and charge variation produced by vertical excitation in the quinolimide
derivatives **1b** and **2b**

Compd[a]	HOMO	LUMO	Δ Charge[b]
1b folded conformation			
1b extended conformation			
2b			

296 [a]Main minimum energy conformers. [b]Charge loss in blue, charge gain in red.

298   We complemented the structural study with NMR experiments, with the aim of proving the

299 influence of the solvent in the conformation of the fluorophores carrying the 2-(dimethylamino)ethyl

300 chain and in their photophysical properties. We compared the ^{1}H-, ^{13}C-, and ^{15}N-NMR spectra of the

301 naphthalimide derivative **1a** in CDCl$_3$ and H$_2$O (Supplementary Material, Table S4). In ^{1}H-NMR the

302 aromatic protons appeared 0.69-1.17 ppm to a lower field in CDCl$_3$ than in H$_2$O. This deshielding

303 could be due to the increase in the π ring current produced by the free electron pair of the

304 dimethylamino nitrogen folded over the ring in CDCl$_3$. However, the dimethyl amino and contiguous

305 protons appeared 0.65 and 0.44 ppm deshielded in H$_2$O with respect to CDCl$_3$, due to charge removing

306 from the free electron pair in its interaction with H$_2$O by hydrogen bond or protonation. In ^{13}C-NMR

307 all the carbons appeared at higher field in D$_2$O than in CDCl$_3$.

308   The assignment of the ^{15}N-NMR spectrum was made based on the ^{1}H,^{15}N correlation HMBC

309   spectrum. Changing from CDCl$_3$ to D$_2$O, the signal of the imidic nitrogen was shielded in 4.5 ppm,

310   while the dimethylamino nitrogen was deshielded in 13.7 ppm. This deshielding is of the same order

311   as described for the protonation of aliphatic tertiary amines (9-18 ppm) [27]. All these results indicated

312   a strong interaction of the dimethylamino group with H$_2$O by protonation or hydrogen bond, which

313   would affect to its conformation and would hinder the PET and increase fluorescence with the solvent

314   acidity.

315   *3.4. H$_2$O and pH sensing and cell imaging*

316   The photophysical features found for the 2-(dimethylamino)ethyl] derivatives **1a** and **1b** –these are

317   a large increase in the fluorescence emission and a red-shift with increasing polarity and acidity of the

318   solvent– make them ideal candidates for fluorescence applications in spectroscopy and imaging.

319   Hence, we next explored the potential use of **1a** and **1b** as H$_2$O and pH sensors. H$_2$O is the most

320   frequent impurity in organic solvents and its detection is crucial in numerous chemical reactions and in

321   industrial applications, such as the fuel industry or raw materials for the food industry [28]. Several

322   naphthalimide-based H$_2$O sensors have been described that function by an ICT mechanism, whose

323   fluorescence decreases when the amount of H$_2$O increases, but none of them function through a PET

324   mechanism [29-31]. To analyze the potential use of **1a** and **1b** as H$_2$O sensors, we determined the

325   sensing performance and the detection limit (LOD)[32] of small amounts of water in CH$_3$CN, by

326   measuring the fluorescence maximum intensities of 18 μM solutions of each fluorophore, to which

327   rising percentages (0-1%) of H$_2$O were added, after excitation at their respective absorption maxima.

328   We employed a relative calibration, focusing on the variation of the quotient F/F_0 versus H$_2$O volume,

329   where F is the experimental emission intensity and F_0 is the reference intensity in the absence of

330   water[33]. This calibration gave a LOD of 0.34% for the naphthalimide derivative **1a** and 0.55% for

331   the quinolimide derivative **1b**.

332   We also studied the pH dependence of the properties of **1a** and **1b**. To minimize the interference

333   of the acidity of solvent in the sensitivity of **1a** and **1b** to pH, this was first studied in CH_3CN with

334   increasing amounts of TFA. As shown in Figure 5, both in **1a** and **1b**, the fluorescence intensity

335   increased sharply with increasing acid concentration, at pH values below 5.5, reaching a maximum

336   with the addition of one equivalent of TFA (pH = 4.9). In the case of the naphthalimide **1a**, the

337   fluorescence remained constant, without falling, until pH<1, but in the quinolimide **1b**, after the

338   maximum, it fell back to a minimum at pH = 1. The increases in fluorescence could be explained by

339   inhibition of the PET, confirming that acidity of the medium can promote switching to an ON state.

340   Interestingly, the decrease in fluorescence bellow pH = 3 in the quinolimide derivative **1b** would be

341   due to protonation of its N_1, which would decrease the intramolecular charge transfer (ICT). These

342   results indicate that **1b** behaves as an OFF-ON-OFF sensor of acidity in organic solvents. However, in

343   H_2O the addition of HCl did not affect the fluorescence emission of **1a**, while in **1b** the fluorescence

344   intensity decreased till a minimum at pH = 1 (Figure S4). These results show that the PET does not act

345   in H_2O, since the solvent itself provides the sufficient stability to the extended conformation to prevent

346   PET, leading to the highly fluorescent form. The addition of further acid to water has no effect in the

347   properties of **1a** and **1b**, except for the protonation of the N_1 in the quinolimide ring of **1b**.
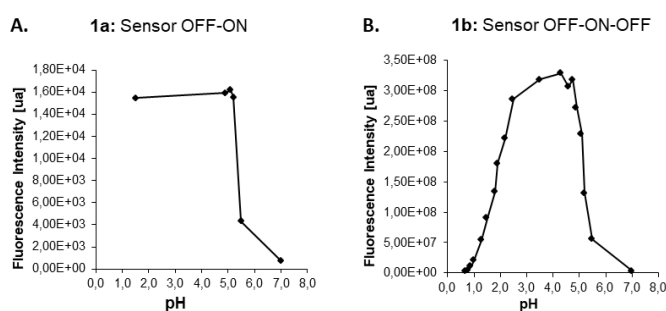
**Figure 5.** Sensitivity of naphthalimide **1a** (A) and quinolimide **1b** (B) to pH in CH_3CN.

348   The number of polarity sensing fluorophores with OFF-ON features when increasing the

349   environment polarity is very limited, including acridine [34], pyrene-3-carboxaldehyde [35], and 7-

350   methoxy-4-methylcoumarin [36], which have restricted application due to quenching of their

351 fluorescence by protonation and to their low excitation and emission wavelengths [37]. The scarcity of

352 this type of fluorophores, which emit in polar media, has limited the monitoring of biological

353 processes that imply an increase in local hydrophilicity. Among the limited examples of this type of

354 sensors, recently, 2-(*trans*-(4-hydroxy)-cyclohexylamino)naphthalimide derivatives have been

355 described as biothiol sensors [38], 2-(2-aminoethyl)-naphthalimide as *in cellulo* metal sensor [13], and

356 BODIPY derivatives as sensors of local hydrophilicity in dysfunctional lysosomes [39]. In view of

357 these precedents and the photophysical behavior of the naphthalimide and quinolimides herein

358 described, we explored their application as *in cellulo* imaging probes in macrophages. These are multi-

359 functional immune cells with key roles in host defense and tissue remodeling, which have been widely

360 studied as models for imaging cellular activity [40-47].

361 Mouse macrophages were treated with a 5 μM concentration of each fluorophore and, after one

362 hour of incubation at 37 °C, the cells were visualized by confocal microscopy. The emission of the

363 derivatives **1a,b** and **2a,b** was observed with a UV filter (350-439 nm), after excitation with a 364 nm

364 laser. As shown in Figure 6, cells treated with the 2-(hydroxyl)ethyl derived fluorophores **2a,b** (Figure

365 6B and F) displayed very low fluorescence, almost as control cells, while cells treated with the 2-

366 (dimethylamino)ethyl derived fluorophores **1a,b** (Figure 6C,D and 6G,H) showed a significant

367 increase in fluorescence, localized at the cytoplasm.
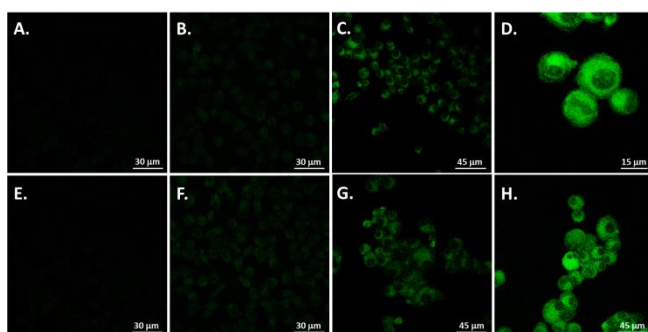
Figure 6. Confocal microscopy of mouse macrophages treated with a 5 μM concentration of LPS and then with **1a,b** and **2a,b** (5 μM). (A, E) Untreated cells; (B) Cells labeled with **2a**; (C, D) Cells labeled with **1a**; (F) Cells labeled with **2b**; (G, H) Cells labeled with **1b**.

368

369

4. Conclusions

The results herein described show that small structural modifications in fluorophores derived from naphthalimides and quinolimides, such as the replacement of a hydroxyl group by a dimethylamino group, can change the character of solvatochromic fluorophores (ICT fluorophores) to reversed solvatochromic ones, with higher emission in polar than in apolar environments, by means of a PET mechanism of charge transfer through space.

In the excited-state, even in less polar solvents, the folded and extended conformation of the dyes coexist. We have estimated and described the kinetics of the excited-state reaction of the 2-(dimethylamino)ethyl substituted naphthalimide **1a** in chloroform to illustrate its conformational dynamics in function of the environment acidity. Due to this dynamics, the folded conformation switches to an extended conformation, giving rise to a red-shifted form. An elegant combination of photophysical measurements with TD-DFT calculations, X-ray analysis and NMR structural studies confirmed such a model. Importantly, the presence of folded and extended conformations allowed the 2-(dimethylamino)ethyl derivatives **1a,b** to switch from PET-quenched dyes in nonpolar solvents to ICT-based probes in polar protic solvents, in contrast with the corresponding 2-(hydroxy)ethyl analogues **2a,b**. This controllable switching mechanism allows tailoring the photophysical properties of PET dyes, providing a way to achieve bright probes in polar and protic solvents that can be used for cytoplasm cell imaging and as H_2O and pH sensors.

Conflict of interest

The authors have no conflicts of interest to declare.

Acknowledgements

20

396

397 **Supplementary Material**

398   Supplementary material to this article can be found online at

399

400 **References**

401 [1] Prasanna de Silva A, Rice TE. A small supramolecular system which emulates the unidirectional,
402   path-selective photoinduced electron transfer of the bacterial photosynthetic reaction center.
403   Chem Commun 1999163-4.

404 [2] Cui D, Qian X, Liu F, Zhang R. Novel Fluorescent pH Sensors Based on Intramolecular Hydrogen
405   Bonding Ability of Naphthalimide. Org Lett. 2004;6:2757-60.

406 [3] Georgiev NI, Bojinov VB, Nikolov PS. The design, synthesis and photophysical properties of two
407   novel 1,8-naphthalimide fluorescent pH sensors based on PET and ICT. Dyes Pigm.
408   2010;88:350-7.

409 [4] Panchenko PA, Fedorova OA, Fedorov YV. Fluorescent and colorimetric chemosensors for cations
410   based on 1,8-naphthalimide derivatives: design principles and optical signalling mechanisms.
411   Russ Chem Rev. 2014;83:155-82.

412 [5] Duke RM, Veale EB, Pfeffer FM, Kruger PE, Gunnlaugsson T. Colorimetric and fluorescent anion
413   sensors: An overview of recent developments in the use of 1,8-naphthalimide-based
414   chemosensors. Chem Soc Rev. 2010;39:3936-53.

415 [6] Banerjee S, Veale EB, Phelan CM, Murphy SA, Tocci GM, Gillespie LJ, et al. Recent advances in
416   the development of 1,8-naphthalimide based DNA targeting binders, anticancer and fluorescent
417   cellular imaging agents. Chem Soc Rev. 2013;42:1601-18.

418 [7] Loving GS, Sainlos M, Imperiali B. Monitoring protein interactions and dynamics with
419   solvatochromic fluorophores. Trends Biotechnol. 2010;28:73-83.

420 [8] Yang Z, Cao J, He Y, Yang JH, Kim T, Peng X, et al. Macro-/micro-environment-sensitive
421   chemosensing and biological imaging. Chem Soc Rev. 2014;43:4563-601.

422 [9] Socher E, Imperiali B. FRET-capture: A sensitive method for the detection of dynamic protein
423   interactions. ChemBioChem. 2013;14:53-7.

424 [10] Zhang H, Wang K, Xuan X, Lv Q, Nie Y, Guo H. Cancer cell-targeted two-photon fluorescence
425   probe for the real-time ratiometric imaging of DNA damage. Chem Commun 2016;52:6308-11.

426 [11] González-Vera JA, Fueyo-González F, Alkorta I, Peyressatre M, Morris MC, Herranz R. Highly
427   solvatochromic and tunable fluorophores based on a 4,5-quinolimide scaffold: novel CDK5
428   probes. Chem Commun 2016;52:9652-5.

429 [12] Prasanna de Silva A, Gunaratne HQN, Habib-Jiwan J-L, McCoy CP, Rice TE, Soumillion J-P.
430   New fluorescent model compounds for the study of photoinduced electron transfer: the influence
431   of a molecular electric field in the excited state. Angew Chem, Int Ed Engl. 1995;34:1728-31.

432 [13] Singharoy D, Chowdhury S, Mati SS, Ghosh S, Chattopadhyay K, Bhattacharya SC.
433   Photoinduced electron transfer switching mechanism of a naphthalimide derivative with its
434   solvatochromic behaviour: An experimental and theoretical study with in cell investigations.
435   Chem - Eur J. 2017;23:16516-24.

436 [14] Adamo C, Barone V. Toward reliable density functional methods without adjustable parameters:
437   the PBE0 model. J Chem Phys. 1999;110:6158-70.

438 [15] Hariharan PC, Pople JA. Influence of polarization functions on MO hydrogenation energies.
439   Theor Chim Acta. 1973;28:213-22.

440 [16] Frisch MJ, Trucks GW, Schlegel HB, Scuseria GE, Robb MA, Cheeseman JR, et al. Gaussian 09.
441   Wallingford, CT, USA: Gaussian, Inc.; 2009.

442 [17] Tomasi J, Mennucci B, Cammi R. Quantum mechanical continuum solvation models. Chem Rev
443   (Washington, DC, U S). 2005;105:2999-3093.

444 [18] Jmol: an open-source Java viewer for chemical structures in 3D. http://www.jmol.org/

445 [19] Dolomanov OV, Bourhis LJ, Gildea RJ, Howard JAK, Puschmann H. OLEX2: a complete
446   structure solution, refinement and analysis program. J Appl Cryst. 2009;42:339-41.

447 [20] Sheldrick G. A short history of SHELX. Acta Cryst 2008;A64:112-22.

448 [21] Sheldrick G. Crystal structure refinement with SHELXL. Acta Cryst 2015;C71:3-8.

449 [22] Cambridge Crystallographic Data Centre. www.ccdc.cam.ac.uk/getstructures

450 [23] Pardo A, Martin E, Poyato JML, Camacho JJ, Guerra JM, Weigand R, et al. N-Substituted 1,8-
451   naphthalimide derivatives as high efficiency laser dyes. J Photochem Photobiol, A. 1989;48:259-
452   63.

453 [24] Catalán J. Toward a generalized treatment of the solvent effect based on four empirical scales:
454   Dipolarity (SdP, a new scale), polarizability (SP), acidity (SA), and basicity (SB) of the medium.
455   J Phys Chem B. 2009;113:5951-60.

456 [25] Adamo C, Barone V. Toward reliable density functional methods without adjustable parameters:
457   the PBE0 model. J Chem Phys. 1999;110:6158-70.

458 [26] Hariharan PC, Pople JA. Influence of polarization functions on MO hydrogenation energies.
459   Theor Chim Acta. 1973;28:213-22.

460 [27] Witanowski M, Stefaniak L, Webb GA. Nitrogen NMR Spectroscopy. Annual Reports on NMR
461   Spectroscopy. London: Academic Press; 1981.

462 [28] Jung HS, Verwilst P, Kim WY, Kim JS. Fluorescent and colorimetric sensors for the detection of
463   humidity or water content. Chem Soc Rev. 2016;45:1242-56.

464 [29] Niu C-G, Qin P-Z, Zeng G-M, Gui X-Q, Guan A-L. Fluorescence sensor for water in organic
465   solvents prepared from covalent immobilization of 4-morpholinyl-1,8-naphthalimide. Anal
466   Bioanal Chem. 2007;387:1067-74.

467 [30] Niu C, Li L, Qin P, Zeng G, Zhang Y. Determination of water content in organic solvents by
468   naphthalimide derivative fluorescent probe. Anal Sci. 2010;26:671-4.

469 [31] Li Z, Yang Q, Chang R, Ma G, Chen M, Zhang W. N-Heteroaryl-1,8-naphthalimide fluorescent
470   sensor for water: Molecular design, synthesis and properties. Dyes Pigm. 2010;88:307-14.

471 [32] Alankar S, Vipin BG. Methods for the determination of limit of detection and limit of quantitation
472   of the analytical methods. Chronicles of Young Scientists. 2011;2:21-5.

473 [33] Miller JN, Miller JC. Statistics and Chemometrics for Analytical Chemistry. Harlow: Pearson,
474   2018.

475 [34] Kellmann A. Intersystem crossing and internal conversion quantum yields of acridine in polar and
476   nonpolar solvents. J Phys Chem. 1977;81:1195-8.

477 [35] Kalyanasundaram K, Thomas JK. Solvent-dependent fluorescence of pyrene-3-carboxaldehyde
478   and its applications in the estimation of polarity at micelle-water interfaces. J Phys Chem.
479   1977;81:2176-80.

480 [36] Seixas de Melo JS, Becker RS, Macanita AL. Photophysical behavior of coumarins as a function
481   of substitution and solvent: Experimental evidence for the existence of a lowest lying $1(n,\pi*)$
482   state. J Phys Chem. 1994;98:6054-8.

483 [37] Uchiyama S, Takehira K, Yoshihara T, Tobita S, Ohwada T. Environment-sensitive fluorophore
484   emitting in protic environments. Org Lett. 2006;8:5869-72.

485 [38] Singha S, Kim D, Roy B, Sambasivan S, Moon H, Rao AS, et al. A structural remedy toward
486   bright dipolar fluorophores in aqueous media. Chemical science. 2015;6:4335-42.

487 [39] Zhu H, Fan J, Mu H, Zhu T, Zhang Z, Du J, et al. d-PET-controlled "off-on" polarity-sensitive
488   probes for reporting local hydrophilicity within lysosomes. Sci Rep. 2016;6:35627.

489 [40] Fernández A, Vendrell M. Smart fluorescent probes for imaging macrophage activity. Chem Soc
490   Rev. 2016;45:1182-96.

491 [41] Li Y, Liu T-M. Discovering macrophage functions using In Vivo optical imaging techniques.
492   Front Immunol. 2018;9:502/1-/20.

493 [42] Yoo JS, Lee S-C, Jow ZY, Koh PYX, Chang Y-T. A Macrophage-Specific Fluorescent Probe for
494   Intraoperative Lymph Node Staging. Cancer Res. 2014;74:44-55.

495 [43] Park S-J, Kim B, Choi S, Balasubramaniam S, Lee S-C, Lee JY, et al. Imaging inflammation
496   using an activated macrophage probe with Slc18b1 as the activation-selective gating target. Nat
497   Commun. 2019;10:1111.

498 [44] Weber M, Mackenzie AB, Bull SD, James TD. Fluorescence-Based Tool To Detect Endogenous
499   Peroxynitrite in M1-Polarized Murine J774.2 Macrophages. Anal Chem. 2018;90:10621-7.

500 [45] Liu Y, Nie J, Niu J, Meng F, Lin W. Ratiometric fluorescent probe with AIE property for
501   monitoring endogenous hydrogen peroxide in macrophages and cancer cells. Sci Rep.
502   2017;7:7293.

503 [46] Wang W, Ning J-Y, Liu J-T, Miao J-Y, Zhao B-X. A mitochondria-targeted ratiometric
504   fluorescence sensor for the detection of hypochlorite in living cells. Dyes and Pigments.
505   2019;171:107708.

506 [47] Yuan L, Wang L, Agrawalla BK, Park S-J, Zhu H, Sivaraman B, et al. Development of
507   Targetable Two-Photon Fluorescent Probes to Image Hypochlorous Acid in Mitochondria and
508   Lysosome in Live Cell and Inflamed Mouse Model. J Am Chem Soc. 2015;137:5930-8.

509